Scientific Research Publishing

International Journal of Astronomy and Astrophysics, 2026, 16(2), 79-93
https://www.scirp.org/journal/ijaa
ISSN Online: 2161-4725
ISSN Print: 2161-4717

Update to Four Estimates of the Dark Matter Warmness

Bruce Hoeneisen

Universidad San Francisco de Quito, Quito, Ecuador
Email: bhoeneisen@usfq.edu.ec

How to cite this paper: Hoeneisen, B. (2026) Update to Four Estimates of the Dark Matter Warmness. *International Journal of Astronomy and Astrophysics*, **16**, 79-93.
https://doi.org/10.4236/ijaa.2026.162006

Received: March 16, 2026
Accepted: May 26, 2026
Published: May 29, 2026

Abstract

Recently it has become possible to obtain the dark matter density $\rho_h(r)$ of dwarf spheroidal galaxies dSph by measuring the line-of-sight velocity of individual stars. Studying 27 dSph we have arrived at the following *tentative* conclusions: i) dark matter is warm, ii) some dwarf spheroidal galaxies are first generation galaxies in the warm dark matter scenario, iii) rotating dwarf irregular galaxies dIrr and spiral galaxies have dark matter halos that are rotating strongly, and iv) the dark matter halo rotation of some dSph is negligible. With this new *tentative* information, in the present study we update four estimates of the dark matter warmness based on dSph density runs $\rho_h(r)$, the mass of first generation galaxies, the distribution of galaxy masses, and from the number density of isolated dwarf galaxies in the Local Field. These four largely independent estimates are consistent with a "standard thermal relic mass" $0.6\text{ keV} \lesssim m_{th} \lesssim 1.6\text{ keV}$, in tension with some of the current limits.

Keywords

Warm Dark Matter, Spheroidal Galaxies, Dwarf Galaxies, Free Streaming, Dark Matter

1. Introduction

If dark matter is warm instead of cold, the power spectrum of density fluctuations becomes cut-off at short wavelengths due to dark matter particle free-streaming, first generation galaxies acquire a finite mass M_{h1}, the number of galaxies per unit volume and mass range decreases at the low mass end, galaxy halos acquire a finite core density ρ_{ch} (if no central black hole) with finite radius r_c, the number density of isolated dwarf galaxies in the Local Field becomes reduced, reionization becomes delayed and the optical depth increases, the formation of low mass galaxies becomes delayed, and the number of satellite galaxies becomes reduced.

Each of these effects offers an opportunity to measure the dark matter warmness.

Recently it has become possible to obtain the dark matter density $\rho_h(r)$ of dwarf spheroidal galaxies dSph by measuring the line-of-sight velocity of individual stars. This dark matter dominates the density $\rho(r)$ of the dSph galaxies. Fitting $\rho_h(r)$ of 27 dwarf spheroidal galaxies [1] we arrive at the following *tentative* conclusions: i) dark matter is warm, ii) some dwarf spheroidal galaxies are first generation galaxies in the warm dark matter scenario, iii) rotating dwarf irregular galaxies dIrr and spiral galaxies have dark matter halos that are rotating strongly, and iv) the dark matter halo rotation of some dSph is negligible. With this new perspective, in the present article we update four published estimates of the dark matter warmness. Each of these estimates depends on assumptions and has its own delicate issues. It is the broad agreement of the four largely independent estimates that gives weight to the conclusion that dark matter is warm. The results of this study may also be applied to other extensions of the standard cold dark matter cosmology ΛCDM that have a power spectrum with a cut-off wavevector k_{fs} [2].

2. Definitions

The mass of a galaxy is often defined as the mass within a radius r_{200} corresponding to a mean galaxy matter density $\langle \rho_m(r < r_{200}) \rangle = 200\Omega_m \rho_{\text{crit}}$. $\Omega_m \rho_{\text{crit}}$ is the present day mean matter density of the universe. We assume that warm dark matter is a noble (*i.e.* not excitable), non-degenerate, non-relativistic, gas of particles of mass m_h that are collisional or collisionless. It is in this scenario that we interpret the dSph data. The "warmness" of this gas may be specified by any of the equivalent parameters $v_{h\text{rms}}(1)$, k_{fs}, m_{th}, m_h or a_{NR}. $v_{h\text{rms}}(1)$ is the comoving root-mean-square of the thermal velocity of the dark matter particles defined as

$$v_{h\text{rms}}(1) \equiv v_{h\text{rms}}(a)\, a. \tag{1}$$

a is the expansion parameter normalized to $a(t_0) = 1$ at the present time t_0. $v_{h\text{rms}}(a)$ is the root-mean-square of the thermal velocity of the dark matter particles when the nearly homogeneous universe has expansion parameter a. $v_{h\text{rms}}(a)$ is proportional to a^{-1}, so $v_{h\text{rms}}(1)$ is an adiabatic invariant. Due to the velocity dispersion $v_{h\text{rms}}(a)$, dark matter particles move into, or out of, density minimums, or maximums, thereby attenuating short wavelength density perturbations. As a result of this dark matter free-streaming, the comoving density fluctuation power spectrum of the ΛCDM cosmology becomes multiplied by a cut-off factor $\tau^2(k)$, where k is the comoving wavevector [3]. We assume that the dark matter particles have a Maxwell distribution of velocities (for a justification of the negative chemical potential of the non-relativistic warm dark matter, see [4]). In this case $\tau^2(k)$ has the form $\tau^2(k) = \exp\left(-k^2/k_{\text{fs}}^2\right)$ [5]. This is our definition of k_{fs}. (Other definitions in the literature are $\tau^2(k_{\text{fs}}) = 1/4$ or 1/2.) The relation between $v_{h\text{rms}}(1)$ and k_{fs} is given by Equation (38) of [5]. Instead of specifying k_{fs}, it is customary in the literature to give the "standard thermal relic mass" m_{th} (of spin 1/2) defined by Equations (6) and (7) of [6]. Note how-

ever, that the dark matter particle mass is model-dependent. For boson dark matter with $N_b = 1$ (assumed to have zero chemical potential while ultra-relativistic) the mass m_h is given by Equation (20) of [1] (see also Equation (26) of [7]). Finally, the expansion parameter a_{NR} at which dark matter becomes non-relativistic, is defined as $a_{\mathrm{NR}} \equiv v_{h\mathrm{rms}}(1)/c$. For convenience, the relation between these parameters is presented in **Table 1**.

Table 1. The warmness of dark matter can be specified by any of the equivalent parameters $v_{h\mathrm{rms}}(1)$, k_{fs}, m_{th}, m_h or a_{NR} defined in Section 2. Their relations are presented in this Table.

$v_{h\mathrm{rms}}(1)$	k_{fs}	m_{th}	m_h	a_{NR}
[m/s]	[Mpc^{-1}]	[keV]	[keV]	[]
25	27.81	4.29	1.39	8.3×10^{-8}
50	13.90	2.30	0.83	1.7×10^{-7}
75	9.27	1.60	0.61	2.5×10^{-7}
100	6.95	1.23	0.49	3.3×10^{-7}
150	4.63	0.85	0.36	5.0×10^{-7}
200	3.48	0.66	0.29	6.7×10^{-7}
300	2.32	0.46	0.22	1.0×10^{-6}
500	1.39	0.29	0.15	1.7×10^{-6}
700	0.99	0.21	0.11	2.3×10^{-6}

3. $v_{h\mathrm{rms}}(1)$ from Dwarf Spheroidal Galaxies

Recently it has become possible to derive the dark matter density $\rho_h(r)$ of dwarf spheroidal galaxies dSph from the observed line-of-sight velocities of individul stars. In [1] we fit the solution of hydrostatic equations to the density runs $\rho_h(r)$ of 27 dSph. The fits minimize a χ^2 by varying three parameters: the density $\rho_h(r_{\mathrm{min}})$ of the first measured point (at $r_{\mathrm{min}} \approx 0.01$ kpc), the variable $v'_{h\mathrm{rms}}(1)/\sqrt{1-\kappa_h}$, and the mass M_{BH} of a possible central black hole. κ_h is the fraction of gravity supported by dark matter halo rotation. We neglect κ_h for some dSph (to be discussed below). The definition of $v'_{h\mathrm{rms}}(1)$ is

$$v'_{h\mathrm{rms}}(1) \equiv \sqrt{3}\sqrt{\langle v_{rh}^2 \rangle}\left(\frac{\Omega_c \rho_{\mathrm{crit}}}{\rho_h(r_{\mathrm{min}})}\right)^{1/3}. \tag{2}$$

$\sqrt{\langle v_{rh}^2 \rangle}$ is the root-mean-square of the radial component of the velocities of the dark matter particles, assumed to be independent of r (see, for example, [8]). The warm dark matter adiabatic invariant $v_{h\mathrm{rms}}(1)$ is obtained from $v'_{h\mathrm{rms}}(1)$ as follows:

$$v_{h\mathrm{rms}}(1) = v'_{h\mathrm{rms}}(1)\frac{\eta\epsilon}{f}. \tag{3}$$

$f = 1$ if dark matter is collisional. For collisionless dark matter, see discussion below. $\epsilon = 1$ if the first generation galaxies formed without relaxation, or $\epsilon < 1$ if there is relaxation. If the dSph has a black hole, then $v'_{hrms}(1)$ becomes dependent on the first measurement at r_{min} so a correction η needs to be applied [1].

Equations (2) and (3) may be understood as follows. Consider collisional warm dark matter, and an observer in a density peak in the early universe. This observer feels no gravity, "sees" warm dark matter expand and then contract to form the core of a galaxy (as shown by hydrodynamical equations [9]). If the contraction is adiabatic, Equations (2) and (3) follow.

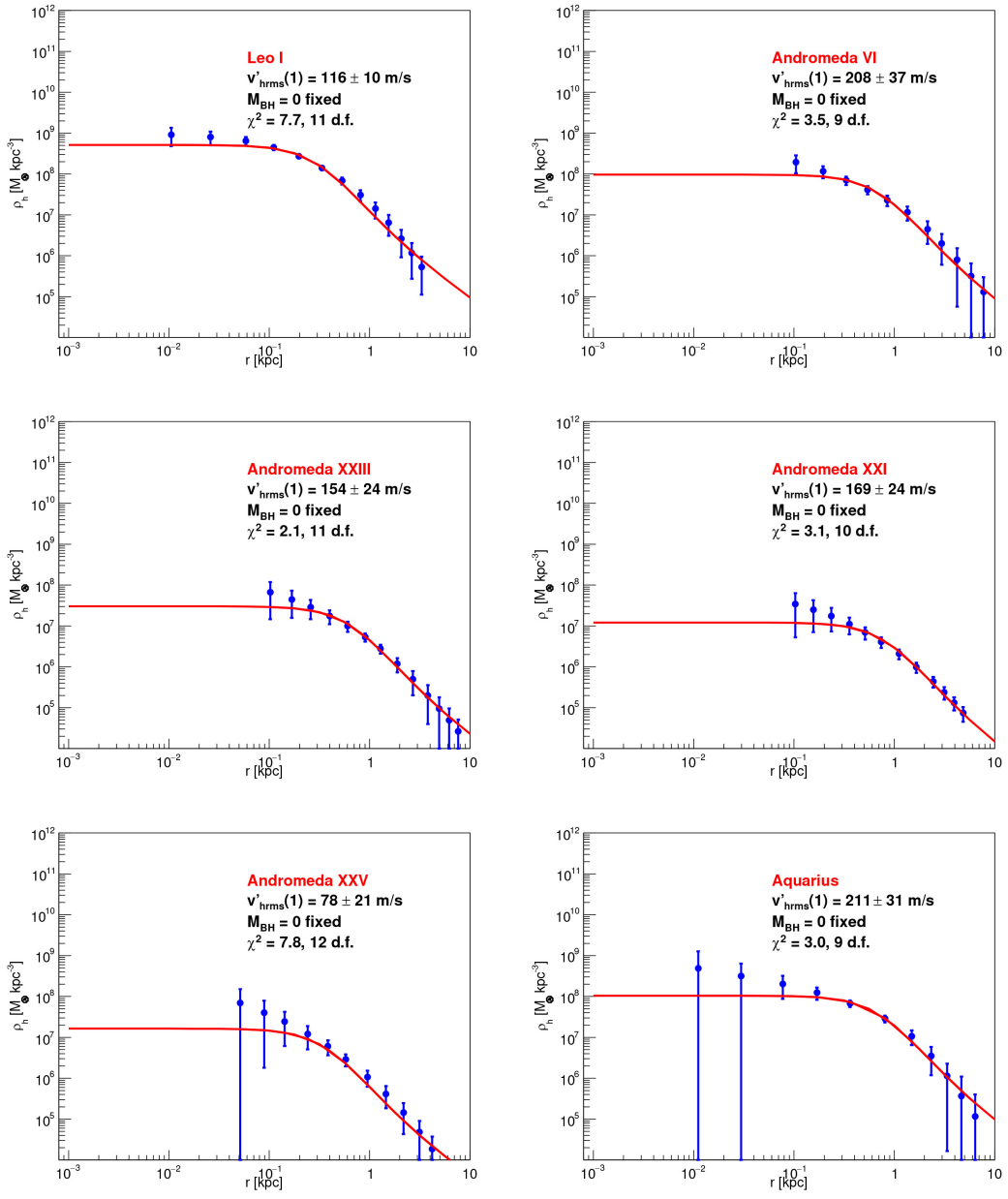

Figure 1. Measured dark matter density $\rho_h(r)$ of dwarf spheroidal galaxies (data from [13]-[17]). The continuous lines are solutions of hydrostatic equations [1] fitted with fixed $M_{BH} = 0$.

A comment on collisional *vs* collisionless dark matter. As and example take a core density $\rho_c = 10^8\, M_\odot / \text{kpc}^3$, core radius $r_c = 0.2$ kpc (see **Figure 1** and **Figure 2**), and, tentatively, a dark matter-dark matter collision cross-section per unit mass $\sigma_{\text{DM-DM}}/m_h = 0.1$ cm²/g (see Table 1 and Figure 13 of [10], and [11]). For this example, $\sqrt{\langle v_{rh}^2 \rangle} = 10$ km/s, and the mean number of collisions of a particle with this velocity and *permanently* in the core (unrealistic) in the age of the Universe is of order 0.3. So dark matter may be significantly collisional if $\sigma_{\text{DM-DM}}/m \approx 0.1$ cm²/g, while $\sigma_{\text{DM-DM}}/m \gtrsim 1$ cm²/g seems to be ruled out (see studies in [11]).

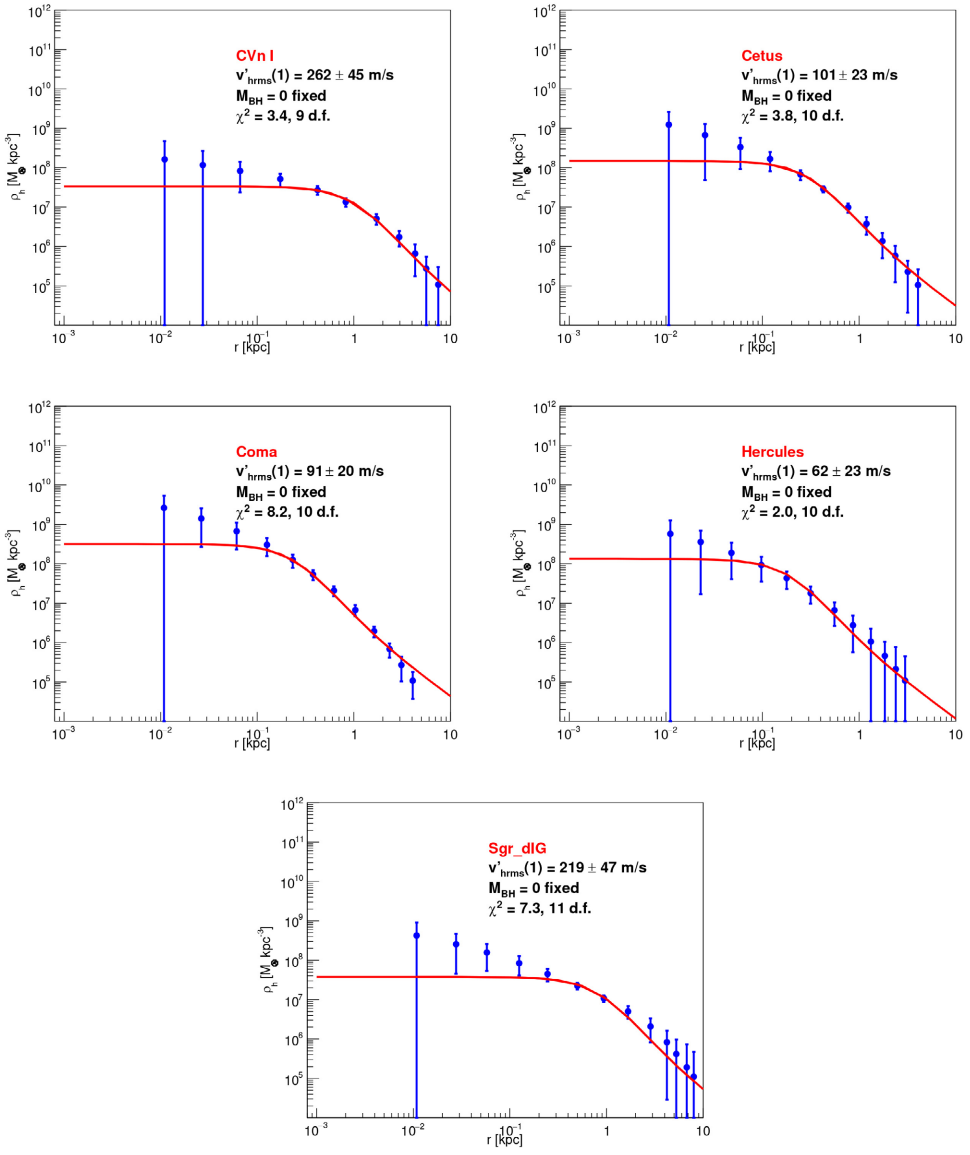

Figure 2. Measured dark matter density $\rho_h(r)$ of dwarf spheroidal galaxies (data from the link https://github.com/koreshk/Estimation-of-phase-space-density-in-dwarf-galaxies on 30 January 2026 given in [17]). The continuous lines are solutions of hydrostatic equations [1] fitted with fixed $M_{\text{BH}} = 0$.

Consider the case of collisionless warm dark matter. In this case $f = x^{1/6}/\sqrt{2\cdot\ln(x)}$, where $x \equiv \rho_c/\rho_{\rm B}$, and the background density is $\rho_{\rm B} = \Omega_c \rho_{\rm crit}/a^3$ (see Appendix of [12]). For example, for galaxies observed at $a = 1, 0.3, 0.1$, $f = 2.2, 1.4, 0.9$, respectively. For our present estimate, we will take, as a bench-mark, $f \approx \sqrt{3}$.

To avoid the uncertainty of η due to the black hole, here we will study a subset of the 27 dwarf spheroidal galaxies that have a black hole mass that is not significantly different from zero, *i.e.* we require that the χ^2 of the fit increase by less than 3 units when $M_{\rm BH}$ is fixed to zero. We also require that the galaxy have $M_h < 10^{10} M_\odot$ (to favor first generation galaxies). This selection leaves 11 dSph. Fitting these 11 dSph with $M_{\rm BH}$ fixed to zero, obtains the results in **Figure 1** and **Figure 2**, and summarized in **Table 2**.

Table 2. For dwarf spheroidal galaxies dSph with black hole mass $M_{\rm BH}$ consistent with zero (see text), and $M_h(<r_{200}) < 10^{10} M_\odot$, we present the stellar mass M_* and neutral hydrogen mass $M_{\rm HI}$ (from the LVDB catalog [18]), and $M_h(<r_{200})$ and $v'_{h\rm rms}(1)/(1-\kappa_h)$ (from the fit with fixed $M_{\rm BH} = 0$). Some entries are not available.

Dwarf	$\log_{10} M_*/M_\odot$	$\log_{10} M_{\rm HI}/M_\odot$	$\log_{10} M_h/M_\odot$	r_{200} [kpc]	$v'_{h\rm rms}(1)/(1-\kappa_h)$
			to r_{200}		[m/s]
Leo I	6.96		9.9	62.4	116 ± 10
Andromeda VI	6.75		9.9	64.1	208 ± 37
Andromeda XXIII	6.14		9.0	32.2	154 ± 24
Andromeda XXI	5.81		8.7	26.1	169 ± 24
Andromeda XXV	5.87		7.9	13.3	78 ± 21
Aquarius	6.42	6.54	9.9	66.8	211 ± 31
CVn I			9.8	56.8	262 ± 45
Cetus	6.71		9.2	35.9	101 ± 23
Coma			9.4	41.7	91 ± 20
Hercules	4.56		8.5	21.2	62 ± 23
Sgr dIG			9.6	49.2	219 ± 47

Let us now discuss dwarf spheroidal galaxy rotation. For baryons, the fraction of gravity supported by stellar rotation with velocity V_{Tb} is $\kappa_b = V_{Tb}^2/\left(2\left\langle v_{rh}^2\right\rangle\right)$. The measured value of κ_b for Draco, Sextans, Umi, Fornax and Sculptor, assuming $\left\langle v_{rb}^2\right\rangle \approx \left\langle v_{rh}^2\right\rangle$, is $\kappa_b \approx 0.3^2/2 = 0.045$, see last column of Table 3 of [21]. See also [22], and Table 1 of [1]. For dark matter we expect $\kappa_h \lesssim \kappa_b$, so neglecting κ_h for our sample of 11 dSph may be justified. The upper panel of **Figure 3** presents measured distributions of $v'_{h\rm rms}(1)/\sqrt{1-\kappa_h}$ for the dSph (red), dwarf irregular dIrr (green) and spiral galaxies (blue). The three distributions in the top panel of **Figure 3** become approximately overlaid if $\kappa_h \approx 0$ for dSph, $\kappa_h \approx 0.90$ for dIrr, and $\kappa_h \approx 0.97$ for spiral galaxies. So our interpretation is that the dark matter halos of dIrr and spiral galaxies are rotating strongly.

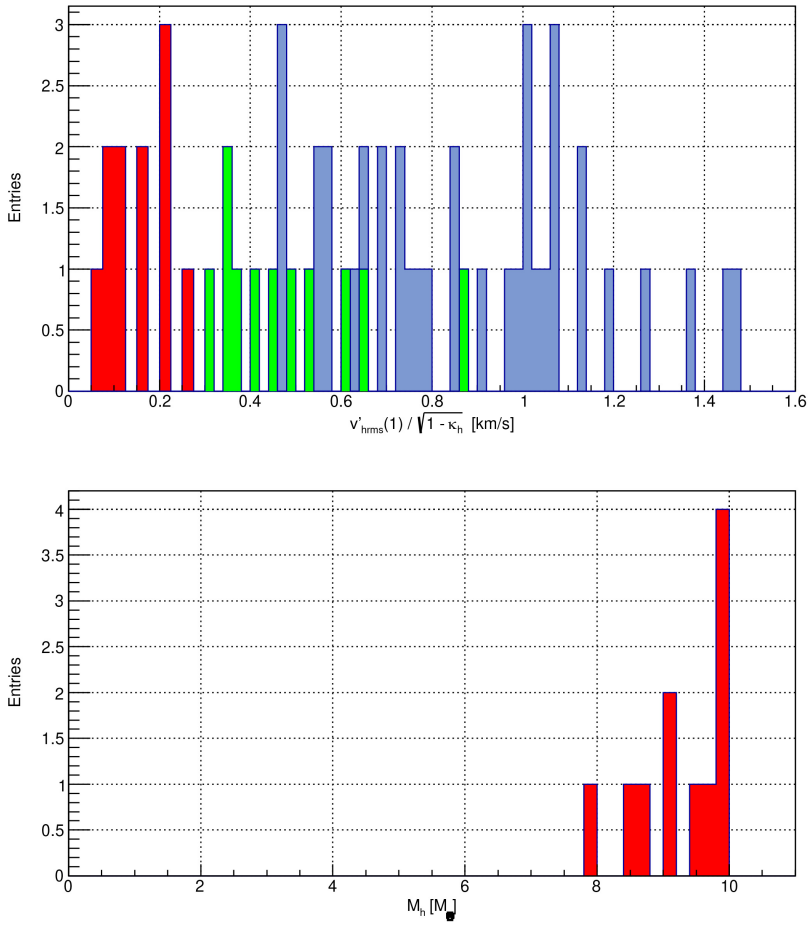

Figure 3. Top: Measurements of $v'_{h\mathrm{rms}}(1)/\sqrt{1-\kappa_h}$. $v'_{h\mathrm{rms}}(1)$ is defined in (2). The distributions correspond to the 11 dwarf spheroidal galaxies dSph from **Table 2** (red), rotating irregular dwarfs dIrr from Figure 2 and Table 2 of [19] (green), and spiral galaxies from Figure 4 and Table A3 of [20] (blue). Bottom: Distribution of the mass M_h of the 11 dwarf spheroidal galaxies (from **Table 2**).

The distribution of the 11 measured $v'_{h\mathrm{rms}}(1)/(1-\kappa_h)$ in **Table 2** with equal weights, has a mean 152 m/s and a standard deviation 64 m/s. This standard deviation is due to residual rotation, and experimental uncertainties. We seek the lower bound of the distribution of $v'_{h\mathrm{rms}}(1)/(1-\kappa_h)$ presented in **Figure 3**, to be able to set $\epsilon = 1$. We *estimate*

$$v_{h\mathrm{rms}}(1) = \frac{1}{f}(120 \pm 60)\,\mathrm{m/s}. \tag{4}$$

For comparison, the estimate in [1] is $v_{h\mathrm{rms}}(1) = (\eta\epsilon/f)\cdot(88 \pm 43)\,\mathrm{m/s}$. Note that we no longer have the correction η due to a central black hole, nor the correction ϵ due to relaxation.

From **Figure 1** and **Figure 2** we observe a tendency of $\rho_h(r)$ to increase at $r \lesssim 0.05$ kpc. If this effect is significant, it may be due to a central black hole, and/or baryons, and/or non-isotropic velocities of collisionless dark matter. If dark matter velocities are not isotropic then there is a tendency of $\rho_h(r)$ to in-

crease at $r \lesssim 0.05$ kpc. To investigate this possibility we define

$$\beta \equiv 1 - \frac{\left\langle v_{\theta h}^2 \right\rangle + \left\langle v_{\phi h}^2 \right\rangle}{2\left\langle v_{rh}^2 \right\rangle}. \tag{5}$$

Now the spherically symmetric non-rotating hydrostatic equations become

$$\frac{1}{r^2}\frac{\mathrm{d}}{\mathrm{d}r}\left(r^2 g_r\right) = -4\pi G\rho_h, \quad \frac{\mathrm{d}\left\langle v_{rh}^2 \right\rangle \rho_h}{\mathrm{d}r} = \rho_h g_r - \frac{2\beta}{r}\left\langle v_{rh}^2 \right\rangle \rho_h. \tag{6}$$

Fits to the data for Leo I, for three values of β (assumed, for simplicity, to be independent of r), are presented in Figure 4. This test shows that the dark matter particle velocities are approximately isotropic, so we should take $f \approx 1$. Note that dark matter may be collisional.

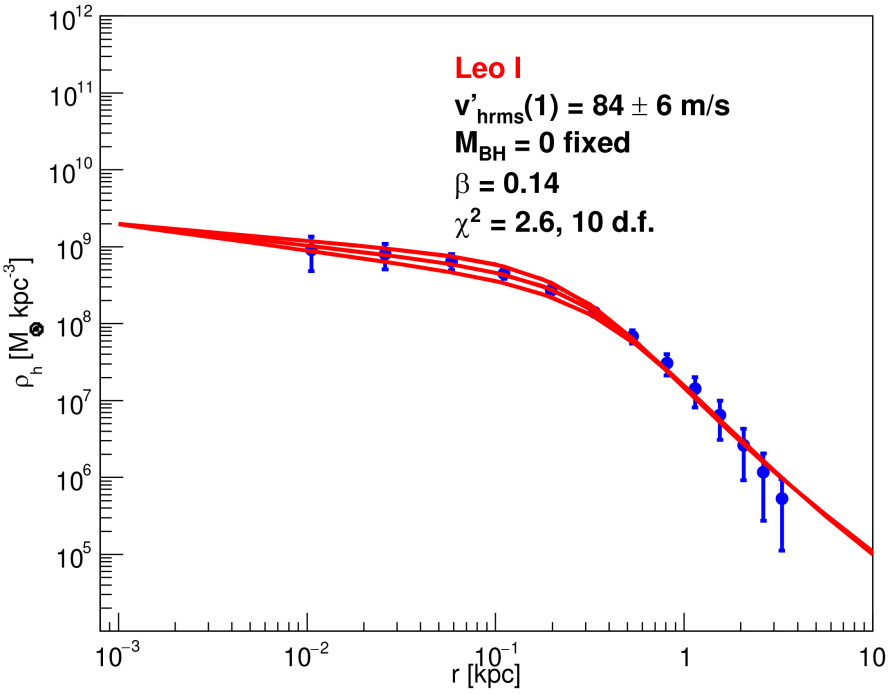

Figure 4. Three fits to the observed $\rho_h(r)$ of Leo I [13] are shown. The fits correspond, from top to bottom, to $\beta = 0.11, 0.14, 0.17$ with $\chi^2 = 14.04, 2.58, 11.79$, respectively, for 11 degrees of freedom. $M_{\mathrm{BH}} = 0$ is fixed. This figure tests the degree of anisotropy of dark matter particle velocities.

4. k_{fs} from the Mass of First Generation Galaxies

Distributions of galaxy mass exhibit a minimum mass M_{h1}. For redshift $z = 3, 4, 5, 6, 7, 8$ the minimum observed $\log_{10}\left(M_{h1}/M_\odot\right)$ is ≈10.9, 8.7, 8.7, 8.7, 8.7, 8.7 respectively [23]. So first generation galaxies appear to have a mass $M_{h1} \approx 5\times 10^8 M_\odot$ or $\log_{10}\left(M_{h1}/M_\odot\right) \approx 8.7$. This minimum M_{h1} is confirmed by Table 2 and Figure 3, so it appears that some dwarf spheroidal galaxies are first generation galaxies in the warm dark matter scenario.

We wish to obtain k_{fs} from M_{h1}. Simulations in [24] obtain

$M_{h1} = 2\times10^{11}, 2\times10^{10}, 2\times10^{9}\,M_\odot$ for $m_{\rm th} = 0.25, 0.5, 1$ keV, corresponding to $k_{\rm fs} = 1.2, 2.6, 5.5$ Mpc^{-1}, respectively. For $M_{h1} = 5\times10^{8}\,M_\odot$ we estimate $k_{\rm fs} \approx 8.7$ Mpc^{-1}, and $m_{\rm th} \approx 1.5$ keV.

As another estimate we use Equation (8) of [25] to calculate the Jeans Mass M_J given $m_{\rm th}$, and then estimate $M_{h1} \approx M_J/2$ (that is not critical, see Figure 2 of [25]). For $M_{h1} = 5\times10^{8}\,M_\odot$ we obtain $m_{\rm th} = 0.77$ keV or $k_{\rm fs} = 4.1$ Mpc^{-1}. (For $M_{h1} = 2\times10^{8}\,M_\odot$ we obtain $m_{\rm th} = 0.98$ keV or $k_{\rm fs} = 5.4$ Mpc^{-1}. For $M_{h1} = 1\times10^{9}\,M_\odot$ we obtain $m_{\rm th} = 0.65$ keV, or $k_{\rm fs} = 3.4$ Mpc^{-1}).

So, from the mass M_{h1} of first generation galaxies in the warm dark matter scenario, we estimate

$$k_{\rm fs} = 6.0 \pm 2.5 \text{ Mpc}^{-1}. \tag{7}$$

The agreement with other determinations of $k_{\rm fs}$ reinforce the conclusion that some dSph may be first generation galaxies in the warm dark matter scenario.

5. $k_{\rm fs}$ from the Galaxy Mass Distributions

The observed stellar mass M_* distributions as well as Press-Schechter predictions, and ellipsoidal collapse extensions, of the halo mass M_h distributions are presented in [23]. The predictions are calculated with a Gaussian window function. The relation between M_* and M_h is assumed to be $M_h/M_* = 10^{1.5}$, independently of M_h. Here we wish to obtain a quantitative estimate of $k_{\rm fs}$ from these distributions.

First we anchor the predictions to the Millenium simulations corresponding to the cold dark matter cosmology ΛCDM at $M_h = 10^{10}\,M_\odot$. From Figure 2 of [26] we obtain, at redshift $z = 5.72$ and $M_h = 10^{10}\,M_\odot$, $\left[M_h^2/\left(\Omega_m \rho_{crit}\right)\right]\cdot {\rm d}n/{\rm d}M_h = 0.022$, corresponding to ${\rm d}n/{\rm d}\log_{10}\left(M_h\right) = 0.20$ dex^{-1}·Mpc^{-3}. Correcting this number from $z = 5.72$ to $z = 6$ obtains ${\rm d}n/{\rm d}\log_{10}\left(M_h\right) = 0.166$ dex^{-1}·Mpc^{-3}. The Millenium simulation assumes $\sigma_8 = 0.90$. We correct to $\sigma_8 = 0.811$ multiplying the power spectrum by (0.811/0.90)^2. The result is ${\rm d}n/{\rm d}\log_{10}\left(M_h\right) = 0.10$ dex^{-1}·Mpc^{-3}, see small red star in **Figure 5**.

Secondly, we consider an improved relation between M_* and M_h which now becomes dependent on M_h. For the star formation efficiency f_* we use Equation (11) of [27] with f_*^0 measured to be in the range 0.5 to 1.0, see Figure 4 of [27]. So at $M_h = 10^{10}\,M_\odot$ we obtain f_* in the range 0.128 to 0.255. So M_* is in the range $M_* \equiv M_h f_* \Omega_b/\Omega_m = 2\times10^{8}$ to $4\times10^{8}\,M_\odot$. Also $\log_{10}\left(M_h/M_*\right)$ is in the range 1.7 to 1.4 (instead of 1.5 in Figure 1 of [23]). So we neglect this correction.

Finally, we switch from the Gaussian window function to the top-hat window function in r-space. We obtain **Figure 5**, calibrated at $M_h = 10^{10}\,M_\odot$ to the ΛCDM Millenium simulation, *i.e.* ${\rm d}n/{\rm d}\log_{10}\left(M_h\right) = 0.10$ dex^{-1}·Mpc^{-3}, and estimate

$$k_{\rm fs} = 3.5 \pm 1.0 \text{ Mpc}^{-1}. \tag{8}$$

Compare in detail with [23].

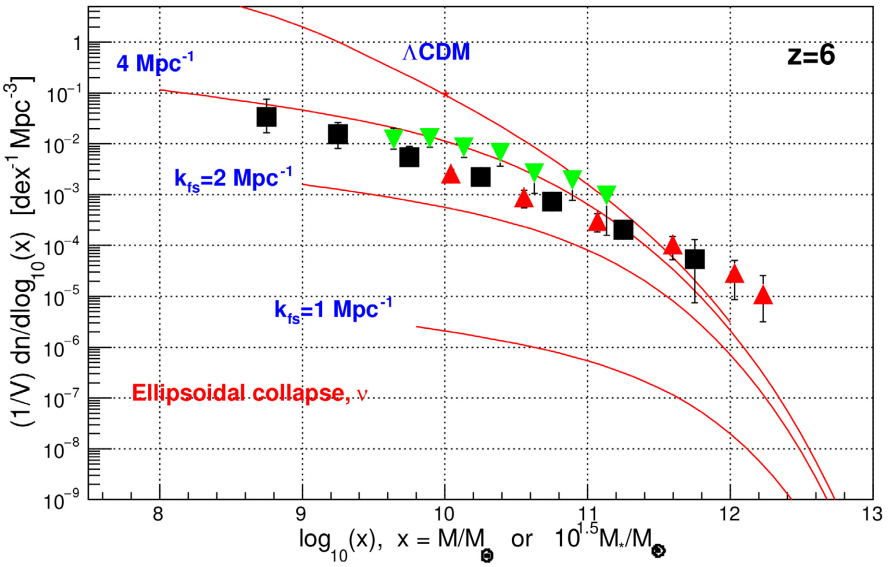

Figure 5. Comparison of predicted and observed distributions of $M_h/M_\odot = 10^{1.5}\, M_*/M_\odot$ at redshift $z = 6$. Stellar mass data are from the Hubble Space Telescope [28] (black squares), from the continuity equation [29] (red triangles), and from the James Webb Space Telescope [30] (green triangles). The predictions are the ellipsoidal collapse extension of the Press-Schechter formalism (Equation (5) of [31] with the top-hat window function in r-space) normalized to ΛCDM at $M_h = 10^{10} M_\odot$ (small red star) as explained in the text.

6. k_{fs} from the Number Density of Isolated Dwarf Galaxies in the Local Field

In [32] we obtain k_{fs} from the number density of isolated dwarf galaxies in the Local Field, *i.e.* within 3 Mpc of the Milky Way, excluding the Milky Way and Andromeda galaxies and satellites. We obtain $k_{fs} \approx 5.6$ before applying a large correction due to the non-linear regeneration of the density fluctuation power spectrum at large wave vector k. This regeneration occurs during the hierarchical formation of galaxies. I now realize that this non-linear regeneration correction should be applied to the universe at large, but not to first generation isolated dwarf galaxies in the Local Field that has a density approximately equal to the mean density of the universe. Consider and overdense region. This overdense region expands slower than a region with the mean density, and hence the comoving wavelength of density fluctuations in the overdense region decreases. This is a cause of the regeneration of the power spectrum at short wavelength or large wave vector. So, for first generation isolated dwarf galaxies in the Local Field, the non-linear regeneration correction should not be applied (only an uncertainty due to the uncertain density of the Local Field needs to be included). Omitting the non-linear regeneration correction in [32] obtains

$$k_{fs} = 5.6^{+1.0}_{-1.4}\ \text{Mpc}^{-1}. \tag{9}$$

7. Cross-Checks

As a cross-check with data, consider Figure 1, Figure 3 and Figure 7 of [33] for

the pseudo-isothermal sphere $\rho_h(r) = \rho_{ch}/\left(1+r^2/r_c^2\right)$. The dark matter temperature-to-mass ratio is $T_h(r_{200})/m_h = (3.6\pm0.5)\times10^{-6}$ K/eV at the "edge" of the halo, *i.e.* at r_{200} defined such that $\rho_h(r_{200}) = 200\rho_{\text{crit}}$. This value of T_h/m_h is also valid in the center of halos with the least mass, *i.e.* $M_h \approx 10^{8.7} M_\odot$ that are not rotating significantly (see Figure 1, Figure 3 and Figure 7 of [33]). Note that for the pseudo-isothermal sphere, $\sqrt{\langle v_{rh}^2 \rangle}$ is approximately independent of r (see Figure 6 of [33]). The corresponding $\sqrt{\langle v_{rh}^2 \rangle}$ is 5300 m/s for the lightest dwarfs with $M_h \approx 10^{8.7} M_\odot$, with non-rotating dark matter halo, and with core density $\rho_c \approx 10^8\, M_\odot/\text{kpc}^3$ (see **Figure 1** and **Figure 2** above). Then the dark matter comoving thermal velocity is $v_{h\text{rms}}(1) \approx 64/f$ m/s. This cross-check with data validates, within a factor ≈2, the measurement method of $v_{h\text{rms}}(1)$ presented in Section 3 for non-rotating first generation galaxies in the warm dark matter scenario.

Cross-check with simulations: The central dark matter densities of the dSph in **Figure 1** and **Figure 2** range from $\rho_{ch} \approx 1\times10^7 M_\odot$ to $\approx 5\times10^8 M_\odot$, or $\rho_{ch}/\rho_{\text{crit}} = 8\times10^4$ to 4×10^6. From Figure 2 of [34] we obtain $m_{\text{th}} \gtrsim 0.13$ keV. From **Figure 1** and **Figure 2** the core radius is $r_c \approx 0.1$ (within a factor ≈2). From Figure 8 of [34] we obtain $0.4\text{ keV} \lesssim m_{\text{th}} \lesssim 1.8\text{ keV}$.

In [32] we obtain k_{fs} from the number density of isolated dwarf galaxies in the Local Field. We repeat that analysis at redshift $z = 7$ that corresponds approximately to the redshift of half-reionization. We vary k_{fs} to obtain the observed number density of galaxies at $z = 7$. The result is $k_{\text{fs}} \approx 7.0\pm1.0$ Mpc^{-1}. One simulation is presented in **Figure 6**. Corrections need to be studied. Nevertheless, k_{fs} can not be very different from ≈7 Mpc^{-1}.

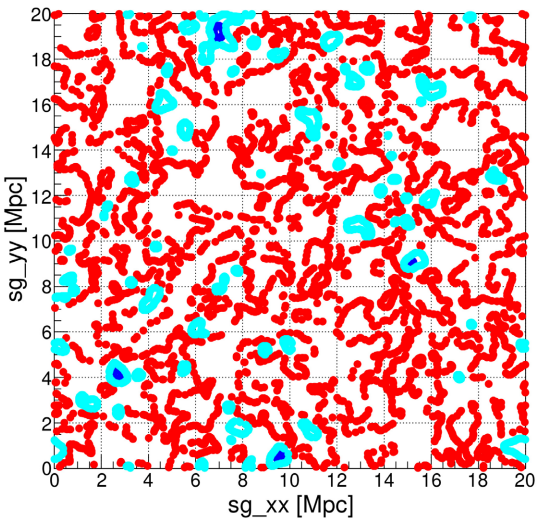

Figure 6. Warm dark matter density $\rho_h(r)$, at redshift $z = 7$ with $k_{\text{fs}} = 7$ Mpc^{-1}, and coordinate sg_zz = 3.3 Mpc, obtained from the comoving power spectrum of density fluctuations $P_{\Lambda\text{CDM}}(k)\exp\left(-k^2/k_{\text{fs}}^2\right)$. The contours of relative overdensity are $\delta = 0$ (red), 1.0 (green), and 1.686 (blue) corresponding to collapsed galaxy halos. For details, see [32].

8. Conclusions

We *tentatively* conclude that some dwarf spheroidal galaxies have negligible dark matter halo rotation, while rotating irregular dwarf and spiral galaxies have dark matter halos that rotate strongly (so rotation may be mainly due to the hierarchical formation of galaxies). We *tentatively* conclude that some dwarf spheroidal galaxies may indeed be first generation galaxies in the warm dark matter scenario. A summary of the four estimates discussed in this article is presented in **Table 3**. These estimates are in disagreement with published limits based on the number of Milky Way satellites, the Lyman-α flux power spectrum, and strong gravitational lensing, summarized in Figure 3 of [35]. Each of these estimates and limits has its own delicate issues, so more studies, measurements and cross-checks are needed to understand the disagreements. Comments on the number of Milky Way satellites, and on the Lyman-α flux power spectrum, are presented in Appendix A and Appendix B. Never-the-less, the broad agreement of these *four largely independent estimates* is evidence in favor of warm dark matter (or other extensions of ΛCDM with a power spectrum with a cut-off wavevector k_{fs}). These estimates allow an extrapolation of the dark matter temperature to the past [1] [7]. The suggestion is that the warm dark matter particles couple to a high-energy extension of the Standard Model of quarks and leptons [1].

Table 3. Summary of four estimates of k_{fs} or $v_{h\text{rms}}(1)$. $f \approx 1$ (see **Figure 4**). These estimates imply $0.6\ \text{keV} \lesssim m_{\text{th}} \lesssim 1.6\ \text{keV}$, see **Table 1**.

k_{fs} [Mpc^{-1}]	$v_{h\text{rms}}(1)$ [m/s]	Comments
$f \times \left(5.8^{+5.8}_{-1.9}\right)$	$(120 \pm 60)/f$	From 11 dSph density runs $\rho_h(r)$, see (4).
6.0 ± 2.5	116^{+82}_{-34}	From the mass M_{h1} of first generation galaxies.
3.5 ± 1.0	199^{+79}_{-45}	From distributions of M_*, see [23] and text.
$5.6^{+1.0}_{-1.4}$	124^{+41}_{-19}	From nmber density in LF, see [32] and text.

Conflicts of Interest

The author declares no conflicts of interest regarding the publication of this paper.

References

[1] Hoeneisen, B. (2026) Warm Dark Matter Properties from Dwarf Spheroidal Galaxy Observations. *International Journal of Astronomy and Astrophysics*, **16**, 25-40. https://doi.org/10.4236/ijaa.2026.161003

[2] Lapi, A., Ronconi, T., Boco, L., Shankar, F., Krachmalnicoff, N., Baccigalupi, C., *et al.* (2022) Astroparticle Constraints from Cosmic Reionization and Primordial Galaxy Formation. *Universe*, **8**, Article No. 476. https://doi.org/10.3390/universe8090476

[3] Boyanovsky, D., de Vega, H.J. and Sanchez, N.G. (2008) Dark Matter Transfer Function: Free Streaming, Particle Statistics, and Memory of Gravitational Clustering. *Physical Review D*, **78**, Article ID: 063546. https://doi.org/10.1103/physrevd.78.063546

[4] Paduroiu, S., Revaz, Y. and Pfenniger, D. (2015) Structure Formation in Warm Dark Matter Cosmologies Top-Bottom Upside-Down. https://arxiv.org/abs/1506.03789

[5] Hoeneisen, B. (2025) The Warm Dark Matter plus Baryon Linear Power Spectrum. *International Journal of Astronomy and Astrophysics*, **15**, 264-281. https://doi.org/10.4236/ijaa.2025.153017

[6] Viel, M., Lesgourgues, J., Haehnelt, M.G., Matarrese, S. and Riotto, A. (2005) Constraining Warm Dark Matter Candidates Including Sterile Neutrinos and Light Gravitinos with WMAP and the Lyman-α Forest. *Physical Review D*, **71**, Article ID: 063534. https://doi.org/10.1103/physrevd.71.063534

[7] Hoeneisen, B. (2024) Measurements of the Dark Matter Mass, Temperature and Spin. *International Journal of Astronomy and Astrophysics*, **14**, 184-202. https://doi.org/10.4236/ijaa.2024.143012

[8] Savchenko, D. and Rudakovskyi, A. (2019) New Mass Bound on Fermionic Dark Matter from a Combined Analysis of Classical dSphs. *Monthly Notices of the Royal Astronomical Society*, **487**, 5711-5720. https://doi.org/10.1093/mnras/stz1573

[9] Hoeneisen, B. (2022) Warm Dark Matter and the Formation of First Galaxies. *Journal of Modern Physics*, **13**, 932-948. https://doi.org/10.4236/jmp.2022.136053

[10] Tulin, S. and Yu, H.B. (2017) Dark Matter Self-Interactions and Small Scale Structure. *Physics Reports*, **730**, 1-57. https://doi.org/10.1016/j.physrep.2017.11.004

[11] Rocha, M., Peter, A.H.G., Bullock, J.S., Kaplinghat, M., Garrison-Kimmel, S., Oñorbe, J., *et al.* (2013) Cosmological Simulations with Self-Interacting Dark Matter—I. Constant-Density Cores and Substructure. *Monthly Notices of the Royal Astronomical Society*, **430**, 81-104. https://doi.org/10.1093/mnras/sts514

[12] Hoeneisen, B. (2025) Warm Dark Matter Studies with Spiral Galaxy Data. *International Journal of Astronomy and Astrophysics*, **15**, 336-355. https://doi.org/10.4236/ijaa.2025.154021

[13] Pascale, R., Nipoti, C., Calura, F. and Della Croce, A. (2025) Leo I: The Classical Dwarf Spheroidal Galaxy with the Highest Dark Matter Density. *Astronomy & Astrophysics*, **700**, A77. https://doi.org/10.1051/0004-6361/202555004

[14] Pickett, C.S., Collins, M.L.M., Rich, R.M., Read, J.I., Charles, E.J.E., Martin, N., *et al.* (2025) Mass Modelling the Andromeda Dwarf Galaxies: Andromeda VI and Andromeda XXIII. *Monthly Notices of the Royal Astronomical Society*, **540**, 1701-1718. https://doi.org/10.1093/mnras/staf796

[15] Collins, M.L.M., Read, J.I., Ibata, R.A., Rich, R.M., Martin, N.F., Peñarrubia, J., *et al.* (2021) Andromeda XXI—A Dwarf Galaxy in a Low-Density Dark Matter Halo. *Monthly Notices of the Royal Astronomical Society*, **505**, 5686-5701. https://doi.org/10.1093/mnras/stab1624

[16] Charles, E.J.E., Collins, M.L.M., Rich, R.M., Read, J.I., Kim, S.Y., Ibata, R.A., *et al.* (2023) Andromeda XXV—A Dwarf Galaxy with a Low Central Dark Matter Density. *Monthly Notices of the Royal Astronomical Society*, **521**, 3527-3539. https://doi.org/10.1093/mnras/stad752

[17] Bezrukov, F., Gorbunov, D. and Koreshkova, E. (2025) Refining Lower Bounds on Sterile Neutrino Dark Matter Mass from Estimates of Phase Space Densities in Dwarf Galaxies. *International Journal of Modern Physics A*, **40**, Article ID: 2540004. https://doi.org/10.1142/s0217751x25400044

[18] Pace, A.B. (2025) The Local Volume Database: A Library of the Observed Properties of Nearby Dwarf Galaxies and Star Clusters. *The Open Journal of Astrophysics*, **8**, Article No. 142. https://doi.org/10.33232/001c.144859

[19] Hoeneisen, B. (2022) Measurement of the Dark Matter Velocity Dispersion with Dwarf Galaxy Rotation Curves. *International Journal of Astronomy and Astrophysics*, **12**, 363-381. https://doi.org/10.4236/ijaa.2022.124021

[20] Hoeneisen, B. (2019) The Adiabatic Invariant of Dark Matter in Spiral Galaxies. *International Journal of Astronomy and Astrophysics*, **9**, 355-367. https://doi.org/10.4236/ijaa.2019.94025

[21] Martínez-García, A.M., del Pino, A., Aparicio, A., van der Marel, R.P. and Watkins, L.L. (2021) Internal Rotation of Milky Way Dwarf Spheroidal Satellites with *gaia* Early Data Release 3. *Monthly Notices of the Royal Astronomical Society*, **505**, 5884-5895. https://doi.org/10.1093/mnras/stab1568

[22] Salucci, P., Wilkinson, M.I., Walker, M.G., Gilmore, G.F., Grebel, E.K., Koch, A., *et al*. (2012) Dwarf Spheroidal Galaxy Kinematics and Spiral Galaxy Scaling Laws. *Monthly Notices of the Royal Astronomical Society*, **420**, 2034-2041. https://doi.org/10.1111/j.1365-2966.2011.20144.x

[23] Hoeneisen, B. (2024) Are James Webb Space Telescope Observations Consistent with Warm Dark Matter? *International Journal of Astronomy and Astrophysics*, **14**, 45-60. https://doi.org/10.4236/ijaa.2024.141003

[24] Schneider, A., Smith, R.E. and Reed, D. (2013) Halo Mass Function and the Free Streaming Scale. *Monthly Notices of the Royal Astronomical Society*, **433**, 1573-1587. https://doi.org/10.1093/mnras/stt829

[25] Benson, A.J., Farahi, A., Cole, S., *et al* (2013) Dark matter halo merger histories beyond cold dark matter – I. Methods and application to warm dark matter. *Monthly Notices of the Royal Astronomical Society*, 428, 1774-1789. https://doi.org/10.1093/mnras/sts173

[26] Springel, V., White, S.D.M., Jenkins, A., Frenk, C.S., Yoshida, N., Gao, L., *et al*. (2005) Simulations of the Formation, Evolution and Clustering of Galaxies and Quasars. *Nature*, **435**, 629-636. https://doi.org/10.1038/nature03597

[27] Lenson, A.J., Farahi, A., Cole, S., Moustakas, L.A., Jenkins, A., Lovell, M., *et al*. (2012) Dark Matter Halo Merger Histories Beyond Cold Dark Matter—I. Methods and Application to Warm Dark Matter. *Monthly Notices of the Royal Astronomical Society*, **428**, 1774-1789. https://doi.org/10.1093/mnras/sts159

[28] Song, M., Finkelstein, S.L., Ashby, M.L.N., Grazian, A., Lu, Y., Papovich, C., *et al*. (2016) The Evolution of the Galaxy Stellar Mass Function at z = 4-8: A Steepening Low-Mass-End Slope with Increasing Redshift. *The Astrophysical Journal*, **825**, Article No. 5. https://doi.org/10.3847/0004-637x/825/1/5

[29] Lapi, A., Mancuso, C., Bressan, A. and Danese, L. (2017) Stellar Mass Function of Active and Quiescent Galaxies via the Continuity Equation. *The Astrophysical Journal*, **847**, Article No. 13. https://doi.org/10.3847/1538-4357/aa88c9

[30] Navarro-Carrera, R., Rinaldi, P., Caputi, K.I., Iani, E., Kokorev, V. and van Mierlo, S.E. (2024) Constraints on the Faint End of the Galaxy Stellar Mass Function at Z ≃ 4-8 from Deep JWST Data. *The Astrophysical Journal*, **961**, Article No. 207. https://doi.org/10.3847/1538-4357/ad0df6

[31] Sheth, R.K., Mo, H.J. and Tormen, G. (2001) Ellipsoidal Collapse and an Improved Model for the Number and Spatial Distribution of Dark Matter Haloes. *Monthly Notices of the Royal Astronomical Society*, **323**, 1-12. https://doi.org/10.1046/j.1365-8711.2001.04006.x

[32] Hoeneisen, B. (2026) Estimate of the Warm Dark Matter Free-Streaming Cut-Off with Isolated Dwarf Galaxies in the Local Field. *International Journal of Astronomy*

and Astrophysics, **16**, 11-24. https://doi.org/10.4236/ijaa.2026.161002

[33] Borzou, A. (2021) Estimation of the Mass of Dark Matter Using the Observed Mass Profiles of Late-Type Galaxies. *Journal of Cosmology and Astroparticle Physics*, **2021**, Article No. 023. https://doi.org/10.1088/1475-7516/2021/08/023

[34] Macciò, A.V., Paduroiu, S., Anderhalden, D., Schneider, A. and Moore, B. (2012) Cores in Warm Dark Matter Haloes: A Catch 22 Problem. *Monthly Notices of the Royal Astronomical Society*, **424**, 1105-1112. https://doi.org/10.1111/j.1365-2966.2012.21284.x

[35] Liu, B., Shan, H. and Zhang, J. (2024) New Galaxy UV Luminosity Constraints on Warm Dark Matter from JWST. *The Astrophysical Journal*, **968**, Article No. 79. https://doi.org/10.3847/1538-4357/ad4ed8

[36] Boera, E., Becker, G.D., Bolton, J.S. and Nasir, F. (2019) Revealing Reionization with the Thermal History of the Intergalactic Medium: New Constraints from the Lyα Flux Power Spectrum. *The Astrophysical Journal*, **872**, Article No. 101. https://doi.org/10.3847/1538-4357/aafee4

[37] Garzilli, A., Magalich, A., Ruchayskiy, O. and Boyarsky, A. (2022) How to Constrain Warm Dark Matter with the Lyman-A Forest. *Monthly Notices of the Royal Astronomical Society*, **502**, 2356-2363. https://doi.org/10.1093/mnras/stab192

Appendix

A. Comment on the Number of Milky Way Satellites

The Milky Way has 67 observed satellites, and counting [18]. Let us take a nominal Milky Way mass $M_{200} \approx 1.2\times10^{12} M_{\odot}$. The Local Field has 55 observed dwarf galaxies, and counting, in a volume 56.5 Mpc^3 [18] [32]. We take a nominal density of the Local Field $\approx 0.2\rho_{\text{crit}}$ [32], corresponding to a Local Field mass $\approx 1.4\times10^{12} M_{\odot}$. If the number of satellites were proportional to mass, we would estimate $55\times1.2\times10^{12}/1.4\times10^{12} = 46$ satellites for the Milky Way. We need to correct this estimate due to the excess average background density of Milky Way satellites compared to Local Field dwarfs. This correction factor can be estimated with simulations as in [32]. In conclusion, the number of Milky Way satellites appears to be consistent, within a factor ≈2, with the observed number of dwarf galaxies in the Local Field, which in turn is consistent with **Table 3**.

B. Comment on the Lyman-α Forest

As shown in **Figure 7** of [36], the observed Lyman-α flux power spectrum has a cut-off starting at $k \approx 0.03\,\text{s/km}$ or $k \approx 2$ Mpc^{-1}. This cut-off is attributed to the temperature of the inter-galactic gas. However, this cut-off is degenerate with the warm dark matter free-streaming cut-off at wavevector k_{fs}, so setting limits at $k_{\text{fs}} \gtrsim 2$ Mpc^{-1} with Lyman-α data is difficult [37]. If the cut-off is due to warm dark matter free-streaming, instead of the inter-galactic gas temperature, we obtain, from **Figure 7** of [36], $k_{\text{fs}} \approx 5.7$ Mpc^{-1}, in agreement with **Table 3**.